# High-Resolution Imaging with Bad Seeing: PKS 1610-771 as a Test Case

*F. COURBIN [1, 2], J.-F. CLAESKENS[1,*]*

*[1] Institut d'Astrophysique, Université de Liège, Belgium; [2] URA 173 CNRS-DAEC, Observatoire de Paris-Meudon*
**Also Aspirant au Fonds National de la Recherche Scientifique, Belgium*

## 1. Introduction

In a previous issue of *The Messenger* (Courbin et al., 1996), we presented NTT subarcsecond images of the luminous quasar PKS 1610-771, together with its spectrum. The analysis of the data (see also Courbin et al., 1997) leads to the plausible conclusion that the quasar is heavily obscured by dust.

PKS 1610-771 has recently been observed in the infrared, but under much poorer seeing conditions (final frame with a FWHM of 1.66″). We use these data to derive the infrared photometry of the quasar and also to detect the IR counterparts of the faint fuzzy objects surrounding the QSO, which were originally discovered in the optical. This is achieved by using the new deconvolution and co-addition algorithm developed by Magain et al. (1997a, b) to combine 6 individual *K′* images.

Since the high-resolution optical images of PKS 1610-771 can provide a check of the co-addition results, we use these data as an example to present a new way of improving spatial resolution, based on the simultaneous deconvolution of several images of the same field.

## 2. Observations – Reduction

The highly luminous quasar PKS 1610-771 was imaged in the infrared *K′* band during the night of the 19th to 20th of August 1996, with IRAC2b, mounted at the f/35 adapter at the 2.2-m ESO/MPI telescope on La Silla. Lens LB was used. The corresponding pixel size projected on the sky is 0.278″, and the field size is 71″.

The airmass of the object in the middle of the exposure was high (∼1.6), and the observing conditions were rather poor (average seeing of 1.66″, and fast variations of the background). Since the target is not much extended, and since the field is not crowded, small (7″) telescope offsets were done between each individual exposure in order to subtract the background. Special attention was paid in order to maintain simultaneously in the field, the quasar together with a nearby bright star, used to determine the Point Spread Function (PSF).

The total exposure time amounts to 540 seconds, and the calibration of the zero point was done by observing the infrared standard star HD 29250 (Van der Bliek et al., 1996).

## 3. Image Co-addition

The IR data consist of 6 individual exposures that need to be optimally combined and sharpened. This can be done in classical ways, just by aligning and averaging the 6 frames. However, a much more efficient method is to deconvolve the images simultaneously. The aim of the process is to find the best deconvolved model, compatible with each of the 6 frames, i.e. within the error bars fixed by the photon noise of each image.

A PSF has to be calculated in order to carry out the deconvolution. Fortunately, a suitable reference star (i.e. comparable in brightness to the QSO) is present on each frame. The good sampling of the data (FWHM ∼ 6 pixels) allows the construction of an accurate PSF. Even if the data are well sampled, Magain et al. (1997a, b) show that deconvolving by the total PSF of the image results in a violation of the sampling theorem and produces the so-called "deconvolution artifacts". In order to avoid this problem, a narrower PSF has to be used. This ensures that the sampling of the deconvolved image is always compatible with all the spatial frequencies it contains. This has two consequences: (1) the shape of the final deconvolved stars is known and (2) one image can be decomposed in a sum of point sources, plus a (deconvolved) diffuse background. In addition, there is no reason for the pixel size of the deconvolved frame to be the same as in the data. This is of particular interest in the case of IR data where numerous dithered frames are usually taken. In order to take full advantage of the dithering between the exposures, we use for the deconvolution a pixel size two times smaller than in the original data. Our final linear pixel size is then 0.278″/2 = 0.139″. We *choose* the final "deconvolved" PSFs as Gaussians with a FWHM of 6 (small) pixels or, equivalently, we *choose* a final "seeing" of 0.83″. This choice allows to compare the results with our NTT *R*-band images which have a seeing of 0.85″. There is in fact no formal limitation to the final resolution, as soon as the sampling of the deconvolved image remains within the limits imposed by the sampling theorem. It is however our experience that low S/N data do not really allow a deconvolution by much more than a factor 2. Once the final FWHM for the deconvolved image is chosen, the nearby star is used to generate the PSF actually needed for the deconvolution process.

In practice, one has to estimate *guess* starting conditions in order to run the deconvolution code. The background component of the model image is initially set to zero. From NTT images, we know that there are 2 point sources in the field considered here. This is the only prior knowledge we use. Guess intensities and centre positions are supplied for these two objects, in each of the six images.

The programme finds the optimal geometrical transformation between the images during the deconvolution process; therefore, no prior alignment of the frames has to be performed. Since each of the 6 frames is considered with its own (narrower) PSF and since the minimisation procedure takes into account the photon noise of each of the 6 images, the result is an optimal combination (with improved seeing and sampling) of the individual data. Both the seeing and S/N ratio of the images are in fact automatically used to weight the individual frames. In addition, the negative pixel values introduced by the background subtraction necessary in the IR, are not set to zero as needed to run traditional deconvolution algorithms; no positivity constraint is necessary. In fact, the data frames are never changed or interpolated, at any moment of the calculation.

The deconvolution procedure minimises the $\chi^2$ between the re-convolved model and the whole data set, with the further constraint that the background part of the deconvolved image is smooth on the length scale of the deconvolved PSF (the one chosen by the user). The solution is considered acceptable only when the 6 residual frames (corresponding to the 6 data frames), in units of the photon noise, show over the whole field a correct statistical distribution, i.e. Gaussian with a zero mean and a standard deviation of 1. The outputs of the procedure are a deconvolved image and a deconvolved background, free of any contamination by the point sources. As an interesting by-product of the programme, the peak intensities and the positions of the point sources are also returned.

## 4. Results – Discussion

The simultaneous deconvolution of our 6 frames yields the images displayed in Figure 1 (panels (2) and (3)).

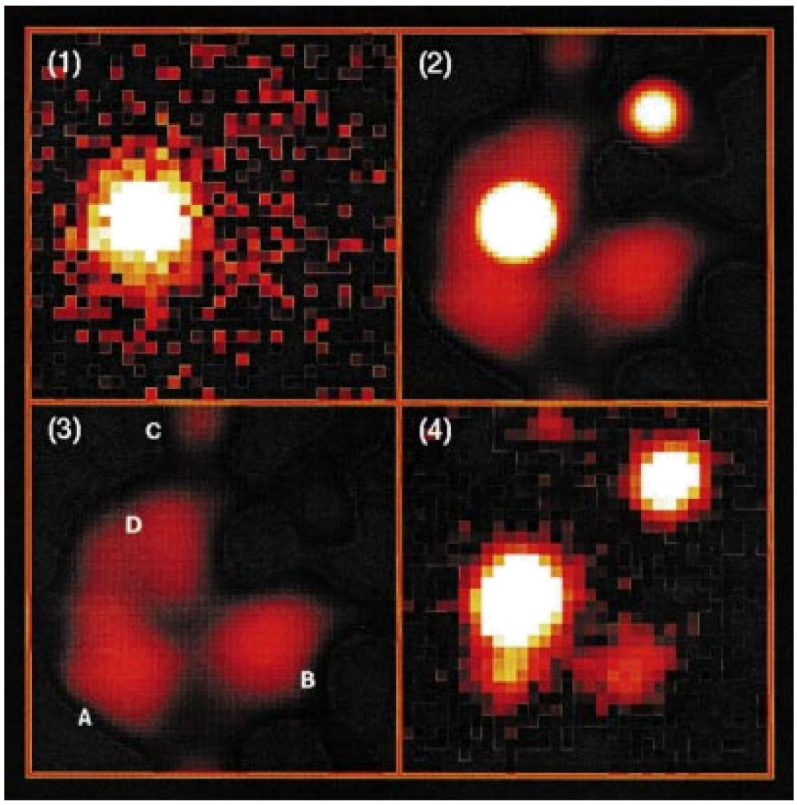


*Figure 1: Comparison of the IR results with high-resolution optical data: field of 6″ × 6″ showing PKS 1610-771. (**1**) Stack of the 6 K′ band images. The seeing is 1.66″. (**2**) Simultaneous deconvolution of the 6 frames. While the original pixel size is 0.278″, it is now 0.139″ and the final FWHM of the deconvolved point sources is 0.83″. (**3**) Deconvolved background showing the faint fuzzy objects hidden by the QSO's light. (**4**) High-resolution R-band NTT image with a seeing of 0.85″ (pixel size of 0.268″), for direct comparison with the IR deconvolved image. Note that the low light levels are fully displayed in all four images, so that any deconvolution artifact would appear, if present.*

The final seeing of our deconvolved IR image is close to the seeing of a reference *R*-band image taken with the NTT +EMMI. It is clear from Figure 1 that objects A, B and C are real: they can be seen on the NTT image. Object D is also real, it appears on the NTT frame after a PSF is subtracted from the QSO's image (see Courbin et al., 1996 and 1997).

From the peak intensities of the point sources, we get the relative photometry of the QSO and the star present in the field. Since the algorithm preserves flux, absolute aperture photometry can be directly performed on the deconvolved image. The *K′* magnitude of the QSO has been independently estimated on the original and deconvolved frames. The two measurements are fully compatible. The deconvolved background is used (panel (3) in Fig. 1) in order to estimate the IR magnitudes of objects A, B, C and D. We have taken the *R* magnitudes from Courbin et al. (1997) to derive the $R-K'$ colour for each object (see Table 1).

*Table 1: Estimated K′ magnitudes and R-K′ colours*

| Object | K′ | R-K′ |
|---|---|---|
| PKS 1610-771 | 15.1 ± 0.1 | 3.1 ± 0.25 |
| STAR | 18.1 ± 0.3 | 1.5 ± 0.35 |
| Gal A | 17.8 ± 0.5 | 3.5 ± 0.60 |
| Gal B | 17.9 ± 0.5 | 3.4 ± 0.60 |
| Gal C | 20.0 ± 0.5 | 3.0 ± 0.60 |
| Gal D | 18.3 ± 0.5 | 4.7 ± 0.60 |
| PSF star | 14.9 ± 0.1 | 1.8 ± 0.10 |

Particular attention has to be paid to the influence of noise on the quality of the deconvolved image. Indeed, in spite of its perfect noise-free aspect, one has to remember that the model is reconstructed from imperfect data. Therefore, the photometry derived from this frame is affected by photon noise, as are the original data. The error bars given in Table 1 are estimated from the integrated photon noise in each object. In addition, we used as a prior knowledge the fact that the QSO and its nearby star companion are point sources. The deconvolution process allows to confirm the QSO as a point source (from the residual frames), but the signal-to-noise ratio in the nearby star image is too low to draw definite conclusions about its precise shape. Star/galaxy discrimination requires better S/N. However, we also performed the deconvolution with only one point source included in the fit (for the QSO). From the resulting deconvolved image, we derive for the star the same $R-K'$ colour than with the former deconvolution.

PKS 1610-771 has a $R-K'$ colour index of 3.1. Using the photographic magnitude from Hunstead and Murdoch (1980), its $B-K'$ is at least 3.8, supporting the hypothesis of strong reddening by dust (Webster et al., 1995). Intrinsic photometric variation of the QSO between the different observations cannot be ruled out, although variations of more than one magnitude would be necessary to significantly change its red colour.

The 4 fuzzy objects close to the QSO have a red $R-K'$ colour index which confirms that they are galaxies. Comparison of the apparent magnitudes and colours of objects A, B and D, with predictions from galaxy evolution models (Pozzetti et al., 1996), leads to the conclusion that they are more likely foreground elliptical galaxies at a redshift between 0.5 and 1.0. Spirals would have been fainter or bluer, at any redshift. Only object C is compatible with a spiral galaxy at $z > 1$.

These data have allowed the determination of the K′ magnitude of PKS 1610-771. The deconvolution process made possible the study of its 4 nearby fuzzy companions, in spite of the rather bad seeing of the IR observations. We have used PKS 1610-771 as a test case because high-resolution images of the object were available to check the validity of a new deconvolution process. We show that relatively good spatial resolution can be achieved even under poor seeing conditions, still keeping the photometric and astrometric properties of the data. The only conditions required for the success of the method are: (1) a good sampling of the original data, (2) a good knowledge of the PSF (which also has to be stable across the field).

## References

Courbin F., Hutsemékers D., Meylan G., Magain P., Djorgovski S.G., 1996, *The Messenger* No. **85**, p. 27.

Courbin F., Hutsemékers D., Meylan G., Magain P., Djorgovski S.G., 1997, *A&A*, **307**, 656.

Hunstead R. W., Murdoch, H. S., 1980, *MNRAS*, **192**, 31 p.

Magain P., Courbin F., Sohy S., 1997a, *The Messenger*, present issue.

Magain P., Courbin F., Sohy S., 1997b, *ApJ*, submitted.

Pozzetti L., Bruzual A.G., Zamorani G., 1996, *MNRAS* **281**, 953.

Van der Bliek N.S., Manfroid J., Bouchet P., 1996, *AAS* **119**, 547.

Webster R.L., Francis P.J., Peterson B.A., Drinkwater M.J., Masci F.J., 1995, *Nature*, **375**, 469.

F. Courbin
courbin@astra.astro.ulg.ac.be